Journal of Biomedical Optics

SPIEDigitalLibrary.org/jbo

Advanced demodulation technique for the extraction of tissue optical properties and structural orientation contrast in the spatial frequency domain

Kyle P. Nadeau
Anthony J. Durkin
Bruce J. Tromberg

SPIE

Advanced demodulation technique for the extraction of tissue optical properties and structural orientation contrast in the spatial frequency domain

Kyle P. Nadeau, Anthony J. Durkin, and Bruce J. Tromberg*
Laser Microbeam and Medical Program, Beckman Laser Institute, 1002 Health Sciences Road, Irvine, California 92612

Abstract. We have developed a method for extracting spatial frequency information content from biological tissue, which is used to calculate tissue optical properties and determine tissue structural orientation. This demodulation method employs a two-dimensional Hilbert transform using a spiral phase function in Fourier space. The approach presented here allows for the determination of tissue optical properties using a single frame of data for each modulation frequency, increasing imaging speed by two to threefold versus conventional, three-phase spatial frequency domain imaging (SFDI). This new single-phase Hilbert transform approach recovers optical property and scattering orientation index values within 1% and 10% of three-phase SFDI, respectively. These results suggest that, using the Hilbert demodulation technique, SFDI data acquisition speed can be increased significantly while preserving data quality, which will help us move forward toward the implementation of a real-time SFDI platform. [DOI: 10.1117/1.JBO.19.5.056013]

Keywords: structural illumination; diffuse optical spectroscopy; wide-field imaging; image processing; Hilbert transform; tissue structural orientation.

Paper 140172R received Mar. 14, 2014; revised manuscript received Apr. 30, 2014; accepted for publication May 5, 2014; published online May 23, 2014.

1 Introduction

The acquisition and analysis of light propagation data in the spatial frequency domain (SFD) allows for a noncontact approach to decouple scattering from absorption in biological tissue, and thus perform quantitative analysis.[1] The first implementation of an SFD technique employed a radially-varying periodic wave as a source.[2] This approach acquires diffuse reflectance measurements taken over several millimeters in the field-of-view and performs Fourier analysis on this data to determine the absorption and reduced scattering coefficients (μ_a and μ_s') at a single point. Since this technique requires diffuse reflectance measurements taken over a wide area in the field-of-view, spatial resolution is limited to a centimeter or greater. An alternative approach was developed, employing a periodic point pattern as a source.[3] In this case, a two-dimensional (2-D) Fourier transform is applied to the entire image, which warrants the determination of optical properties at each pixel in the image, resulting in a scan-free method for generating μ_a and μ_s' maps. Additionally, this approach overcomes the limit in spatial resolution associated with the spatial sampling of reflectance data employed in the first technique. However, there are issues associated with using pencil beam patterns. For example, light detected close to a pencil-beam source is likely to saturate an imaging camera, whereas light detected further away is likely to be attenuated and thus susceptible to noise.

An imaging modality known as spatial frequency domain imaging (SFDI) has been developed, which employs sinusoidal patterns of spatially modulated light as an excitation source.[4,5] In a similar fashion to the previous approaches, diffusely reflected light is analyzed in the SFD to decouple μ_s' from μ_a. The use of sinusoidal patterns of light as a source mitigates the dynamic range issues associated with pencil-beam sources by providing more uniform illumination to the field-of-view. SFDI has been used to evaluate absolute changes in tissue chromophores such as oxy/deoxy-hemoglobin, water, and structural parameters such as μ_s' spectra for a variety of tissue types including skin,[6] brain,[7] and kidney.[8]

Current SFD approaches are limited with respect to the speed at which data can be acquired. In particular, conventional SFDI employs a demodulation method requiring a total of three frames of data for each modulating (AC) spatial frequency.[4,5] These frames correspond to sinusoidal pattern phase offsets of 0, 120, and 240 deg and are combined to extract information content at each AC spatial frequency. The need for having three frames of data taken at each AC spatial frequency limits the speed at which SFDI data can be acquired and is one of the primary bottlenecks preventing the implementation of a real-time SFDI platform. This limitation in data acquisition speed in SFDI translates to a limit in the rate at which we can probe temporal dynamics and amplifies the effects of motion on our measurements.[9] Thus, we are seeking ways to reduce the data acquisition time of SFDI by using fewer frames of data, while at the same time preserving information content. A technique to reduce SFDI data acquisition time was recently developed by Vervandier and Gioux,[10] requiring a single frame of data to map μ_a and μ_s'. This approach applies a one-dimensional Fourier transform to each row or column in an SFDI intensity image and divides the resulting spectrum into a DC component

*Address all correspondence to: Bruce J. Tromberg, E-mail: bjtrombe@uci.edu

0091-3286/2014/$25.00

and an AC component. Although this approach reduces data acquisition time greatly, there may be some loss of information content associated with dividing the spatial frequency spectrum into two components.

In this work, we describe a method that attempts to optimize the tradeoff between data acquisition speed and image quality. This approach relies on a variant of a 2-D Hilbert transform by employing a complex-valued spiral phase function in Fourier space. In this case, only a single frame of data is required for each AC spatial frequency, resulting in an increase in data acquisition speed. Additionally, using the spiral function allows for the extraction of spatial frequency information content from rotated sinusoidal patterns which are used to elucidate tissue structural orientation in the SFD, measured by the scattering orientation index (SOI).[11] We show agreement between our new technique and conventional, three-phase SFDI by comparing diffuse reflectance maps taken at several spatial frequencies from a tissue-simulating phantom, μ_a and μ_s' maps taken from the volar forearm of a human subject, and SOI maps taken from structural orientation phantoms at various orientation angles. Our results show that SFDI data acquisition speed for mapping μ_a and μ_s' can be increased by two to threefold using the proposed technique, depending on the number of AC spatial frequencies used. Additionally, we show that the data acquisition speed for probing tissue structural orientation can be increased threefold.

2 Materials and Methods

2.1 *Spatial Frequency Domain Imaging*

SFDI instrumentation, data acquisition, and data analysis have previously been described in detail.[5] Briefly, structured light is projected onto a sample using a spatial light modulator (SLM), and a camera detects the diffusely reflected light emitted from the boundary of the sample. In three-phase SFDI, three frames of data are acquired at relative modulation phases of 0, 120, and 240 deg for each AC spatial frequency. These phase-offset images are applied to a simple formula to extract the AC information content pixel-by-pixel, as shown in Eq. (1). A simulation of this demodulation approach using three phase-offset modulation patterns is shown in Fig. 1. All data processing and computation used to produce figures were performed using the MATLAB® software suite (MATLAB and Statistics Toolbox Release 2011b, The MathWorks, Inc., Natick, Massachusetts).

$$\mathrm{AC}(x,y) = \frac{2^{1/2}}{3}\{[I_{0^\circ}(x,y) - I_{120^\circ}(x,y)]^2 + [I_{120^\circ}(x,y) - I_{240^\circ}(x,y)]^2 + [I_{240^\circ}(x,y) - I_{0^\circ}(x,y)]^2\}^{\frac{1}{2}}. \quad (1)$$

Next, the demodulated intensity data from the sample is calibrated to that of a tissue-simulating phantom having known

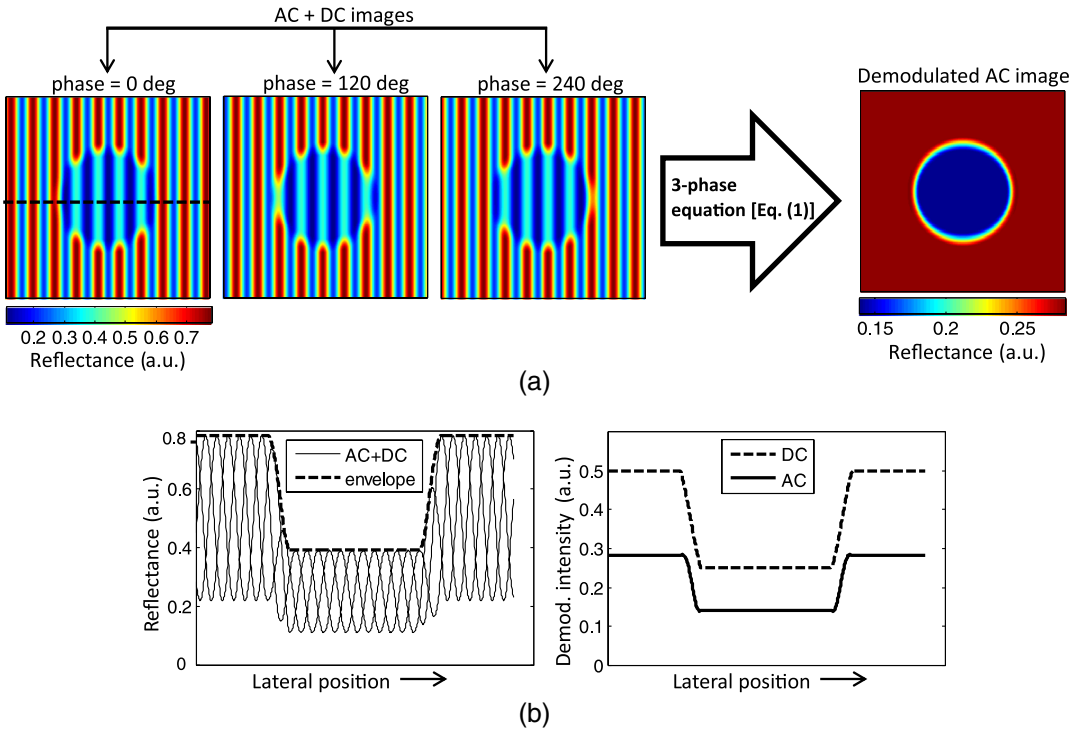

Fig. 1 (a) Simulation of three-phase demodulation technique on a turbid sample with uniform scattering and a circular absorbing lesion in the center of the field of view. Images are acquired at relative modulation phases of 0, 120, and 240 deg. These images are then applied to a three-phase demodulation formula [Eq. (1)], which extracts the AC information content from the sample pixel-by-pixel. (b) Plot of reflectance cross-sections taken from the center row (dashed line shown in a) of each AC + DC image, and the resulting AC + DC information envelope (left). A cross section of the demodulated DC (taken from additional planar image) and AC information content (right) is also shown. The DC cross section is more sensitive than AC to absorption, whereas the AC cross section is more sensitive than DC to scattering.

optical properties. This calibrated diffuse reflectance data at each spatial frequency is then applied to a light transport model such as diffusion or Monte Carlo, from which μ_a and μ_s' maps are determined. Finally, these maps are generated at several wavelengths and are fit to known chromophore spectra to quantitatively determine the concentration of relevant chromophores in the sample.

In order to decouple scattering from absorption, at least two spatial frequencies are required. In the case where the minimal number of frames are taken, 0 (planar illumination) and 0.2 mm^{-1} are typically used. Since there is no spatial variation in the spatial modulation pattern at 0 mm^{-1}, only one phase is required, so a minimum of four frames (per wavelength) total are needed in three-phase SFDI, consisting of a single DC frame and three phase-offset AC frames. After demodulation, a fast lookup table is employed to determine μ_a and μ_s'. The primary limitation with respect to the implementation of real-time SFDI is data acquisition time. In particular, as we currently practice the technique, the need to acquire three frames of data for each AC spatial frequency limits the speed of SFDI data acquisition. We have developed a technique to address this bottleneck by reducing the number of frames required for each modulating frequency from three to one.

2.2 *Two-Dimensional Hilbert Demodulation Technique*

The Hilbert transform is a ubiquitous tool in signal processing with a wide variety of applications in the communication field.[12] The general principle is that a modulating double-sideband signal such as a sine or a cosine contains redundant information; only one sideband is needed to extract the modulated information content. Using the Hilbert transform, one can derive a single-sideband expression for this modulated signal with no loss of information. This single-sideband expression allows for the extraction of the demodulated information content and phase map of the modulated signal. Recently, the concept of applying the Hilbert transform using spiral phase functions in 2-D Fourier space to demodulate 2-D curved patterns in space was developed by Larkin et al.[13,14] We have adopted the general concept of this approach and have applied it to the SFDI workflow.

The modulated reflectance images obtained in SFDI can be described by Eqs. (2) and (3), where $f_{x,y}$ is the modulating spatial frequency, and $\varnothing_{x,y}$ is the phase.

$$I(x,y) = 0.5 * R_{\mathrm{DC}}(x,y) + 0.5 * M(x,y), \tag{2}$$

where

$$M(x,y) = R_{\mathrm{AC}}(x,y) * \cos\{2\pi f_{x,y} + \varnothing_{x,y}\}. \tag{3}$$

The purpose of demodulation is to extract the AC diffuse reflectance term $R_{\mathrm{AC}}(x,y)$ from the detected amplitude $I(x,y)$. Using Euler's theorem, a cosine function can be expressed as the sum of two complex exponentials or sidebands in the frequency domain. As mentioned previously, the Hilbert transform is used to obtain a single-sideband expression for a double-sideband function such as a cosine. Since a single-sideband function can be expressed as a complex exponential, demodulation is straightforward. The magnitude of the single-sideband expression for SFDI modulation results in the diffuse reflectance we wish to obtain.

Our new SFDI demodulation approach employs a 2-D Hilbert transform to SFDI frames by applying a spiral phase function to the image in 2-D Fourier space. One unique aspect of this approach is that it can demodulate frames whose modulation patterns are rotated or arbitrarily oriented. That is, the wavenumber of the modulating pattern can have arbitrary directionality with respect to the lateral imaging axes (x,y). The spiral function is described in Eq. (4)

$$S(u,v) = \frac{u + iv}{\sqrt{u^2 + v^2}}, \tag{4}$$

where u and v are the lateral coordinates in 2-D Fourier space.

In order to implement the Hilbert demodulation technique, the following steps are performed. First, the DC component of the spatially modulated image which consists of both AC and DC components [$I(x,y)$ from Eq. (2)] is removed. A 2-D fast Fourier transform (FFT) is then applied to the resulting AC image [$M(x,y)$ from Eq. (2)]. In 2-D Fourier space, the transformed AC image is multiplied by a map generated using Eq. (4), having the same dimensions as the AC image. Next, an inverse FFT is applied to this product. The resulting image is similar to the original AC image, except that the modulating "cosine" is now a "sine," i.e., the phase of the modulating wave is shifted by 90 deg. Then, the magnitude of this "sine" image is taken, which accounts for the complex contribution of the transformed map due to the orientation angle of the modulating wave, shown in Eq. (4). The resulting term, $H(x,y)$, represents the Hilbert transform of the original AC image [$M(x,y)$]. Finally, $H(x,y)$ is multiplied by the complex unit and added to the AC component of the original AC image. The resulting magnitude is the demodulated AC diffuse reflectance, denoted in Eq. (5) by $R(x,y)$

$$R(x,y) = |M(x,y) + iH(x,y)|, \tag{5}$$

where

$$H(x,y) = |\mathrm{FFT}^{-1}\{\mathrm{FFT}[M(u,v)] * S(u,v)\}|. \tag{6}$$

A walkthrough of the Hilbert technique is shown in Fig. 2 using a simulated DC and AC + DC image. In this simulation, the sample is highly reflective, such that the sinusoidal pattern is kept intact as the light reaches the boundary of the sample. In reality, we apply this technique to turbid tissue simulating samples or biological samples, which will be demonstrated in the experimental results, but this virtual sample was chosen to clearly illustrate the Hilbert demodulation concept. We expect that the Hilbert technique will yield results comparable in quality to those shown in Fig. 2 so long as the reflected modulation pattern is greater in amplitude than the camera noise. This constraint should typically be satisfied when looking at biological samples.

Here, we begin with a DC image at a uniform intensity of one, and an AC + DC image [Eq. (2)] with an intensity varying from zero to one, with a modulation pattern oriented diagonally. First, the DC component is removed from the AC + DC image, and an FFT is performed on the resulting AC image. Next, the spatial frequency map of the transformed AC image is multiplied with the complex spiral function map. The resulting map is then FFT inverted, and the magnitude is taken. This "magnitude" image is then multiplied by the imaginary unit and added to the initial AC image (before Hilbert transform). The magnitude of this sum results in the demodulated AC diffuse reflectance, which is uniform at an intensity of ~0.5.

It should be noted that the demodulated AC images obtained in Fig. 1 and subsequent figures using the Hilbert technique

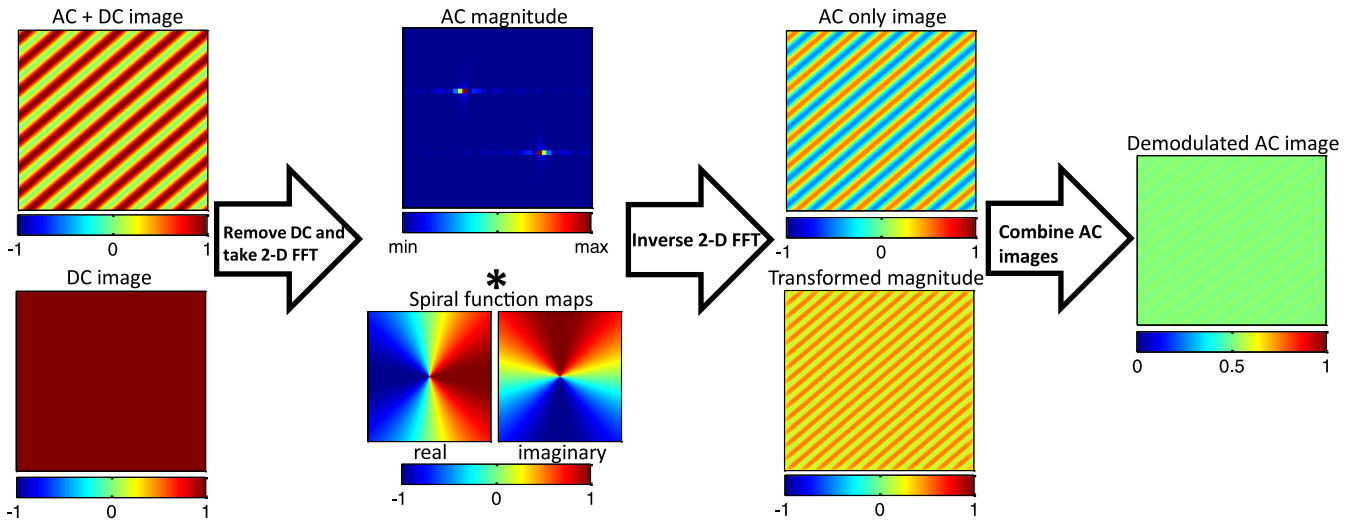

Fig. 2 Simulation of the two-dimensional (2-D) Hilbert demodulation method on a highly reflecting surface. First, the DC component of the modulated image is removed, and a fast Fourier transform (FFT) is performed on the AC + DC image. The resulting 2-D map in Fourier space is then multiplied by a spiral phase function, consisting of a continuous, radially-varying map ranging in value from −1 to +1 in real and imaginary space. An inverse FFT is performed on the map, resulting in an image whose magnitude is the original modulated image phase-shifted by 90 deg. This image is multiplied by the imaginary unit and added to the original image. The magnitude of this image results in the demodulated diffuse reflectance of the AC component from the original AC + DC image.

contain residual ringing artifacts, which are due to the fact that the spatially projected sinusoidal patterns are cutoff by the boundaries of the image and are, therefore, finite in length. We refer to the degradation in image quality as resulting from ringing artifacts. In theory, these artifacts should increase in severity as the number of periods in the modulation pattern in the image decreases. Therefore, one potential strategy to minimizing these artifacts, particularly at lower spatial frequencies, is to use an SFDI instrument having a large field-of-view. Alternatively, a window function such as a Gaussian or Hamming filter could be applied to the image in postprocessing,[15] which will be the subject of future work.

We performed a side-by-side comparison of our advanced Hilbert demodulation technique to three-phase demodulation. To generate the data used to produce the images analyzed in this section, we employed a clinical SFDI system at a wavelength of 658 nm. This system has been described previously.[16] In our first experiment, we compared diffuse reflectance maps obtained on a tissue-simulation phantom at multiple spatial frequencies. This phantom consists of a silicone foundation consisting of India ink as an absorbing agent and titanium dioxide as the scattering agent. The fabrication technique used to make these phantoms has been described previously.[17] Next, we compared μ_a and μ_s' maps extracted from an *in vivo* human forearm. Finally, we evaluated SOI maps taken on a structural orientation phantom consisting of a silicone-based bottom layer (described above), and a top layer composed of sections of pleated air filters at various orientation angles. The SOI of these phantoms has been previously evaluated.[11]

3 Results

3.1 *Tissue Phantom Reflectance Experiment*

Demodulation in the SFDI workflow allows for the extraction of information content in the SFD, which is used to generate μ_a and μ_s' maps. Figure 3 shows a comparison between three-phase SFDI and the Hilbert technique of demodulated diffuse reflectance maps of a homogeneous tissue-simulating phantom. Maps of demodulated reflectance at an AC spatial frequency of 0.2 mm^{-1} are shown in the figure. Here, only the first phase (0 deg) intensity image is applied to the Hilbert technique, whereas intensity images at three phases (0, 120, and 240 deg) are applied to three-phase demodulation [shown in Eq. (1)]. Average demodulated diffuse reflectance results are shown at five spatial frequencies evenly distributed from 0 to 0.2 mm^{-1} which is taken from the region of interest (ROI) shown in the black box. These spatial frequencies are typically employed in the SFDI workflow, and instrumentation and models have been shown to perform adequately in this range.[5,18] Here, we see good demodulation quality across the entire field-of-view, with pixel intensity differences between three-phase and Hilbert generally within 5%. We also show agreement in diffuse reflectance values between the two techniques, with mean reflectance values within 1% within the ROI for spatial frequencies of 0.05, 0.1, 0.15, and 0.2 mm^{-1}. It should be noted that, although the sample in this case is homogeneous, the reflectance intensity over the field-of-view is not. This is due to the inhomogeneity of the light source, which is accounted for during calibration.

Accurate demodulation, and thus determination of AC information content in the SFD, is a necessary component of SFDI and is what allows for the generation of μ_a and μ_s' maps. In the following section, we present μ_a and μ_s' maps extracted from a volar forearm using the Hilbert demodulation technique and compare this data directly to μ_a and μ_s' maps derived using three-phase demodulation.

3.2 *In Vivo Volar Forearm Experiment*

Optical property maps of a human volar forearm were calculated using a fast lookup table method, employing spatial frequencies of 0 and 0.2 mm^{-1}. Figure 4 shows a comparison of μ_a and μ_s'

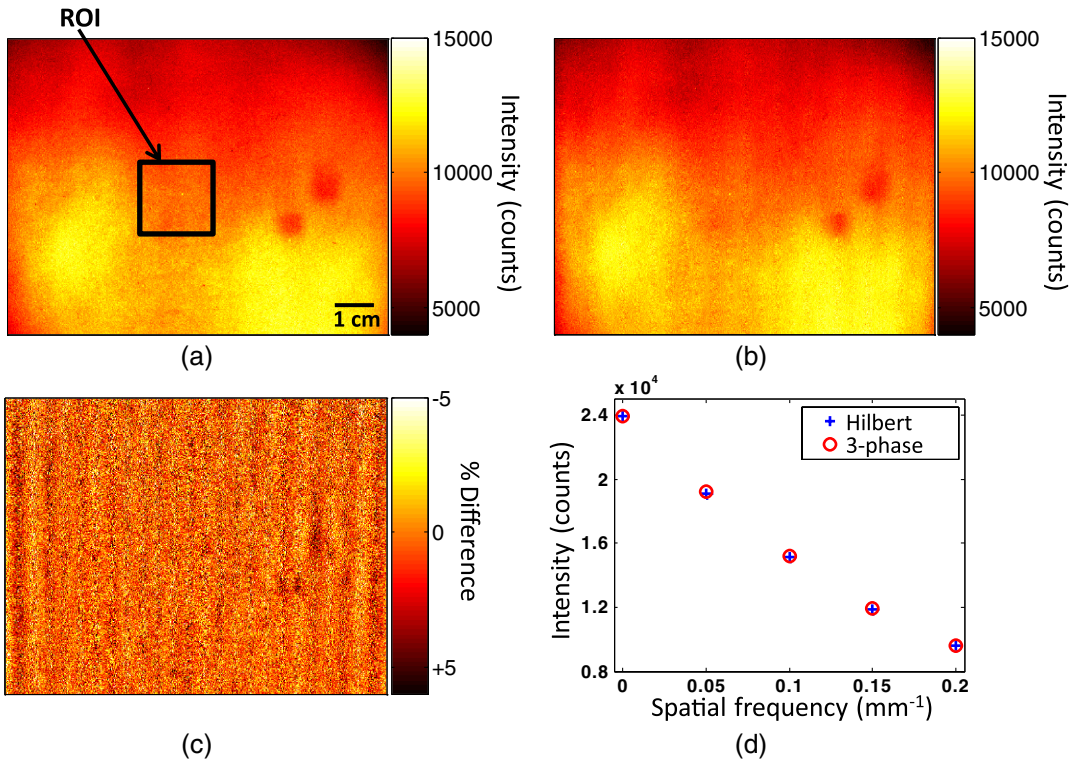

Fig. 3 Demodulated reflectance images at 0.2 mm^{-1} of a tissue-simulating phantom using (a) conventional, three-phase spatial frequency domain imaging (SFDI) (4 frames), and (b) the advanced, Hilbert-based technique (2 frames). (c) Map of percent difference in demodulated reflectance between three-phase SFDI and the Hilbert-based technique. (d) Plot of mean diffuse reflectance versus spatial frequency for the region of interest (ROI), shown in (a).

maps of the forearm using the three-phase (left column) and Hilbert (right column) demodulation techniques. Here, we see agreement in optical property values between the two techniques, with the difference in mean μ_a and μ_s' values in the ROI (shown in the black box) being 0.2% and 0.15%, respectively.

A key motivation for spatially modulating light in SFDI is to decouple scattering from absorption. Therefore, quantitative optical property mapping is an essential feature of the technique. Figure 4 demonstrates the ability of our new demodulation technique to produce μ_a and μ_s' maps in biological tissue that agree with the conventional demodulation method, which suggests that we can reduce this new technique to practice. The payoff using the new Hilbert technique is the reduction in frames of data required to derive μ_a and μ_s', and thus an increase in data acquisition speed. In the case shown in Fig. 4, the number of frames reduced using the Hilbert technique over a three-phase demodulation is from four to two, resulting in a twofold increase in imaging speed. However, the payoff in speed increases further if more spatial frequencies are employed, asymptotically approaching a threefold increase.

Although the primary benefit of using the Hilbert technique over a three-phase demodulation is the increase in imaging speed, there are additional benefits. In particular, as shown in Fig. 2, the Hilbert technique can demodulate rotated or oriented sinusoidal patterns using only one AC phase. Acquiring reflectance data at multiple sinusoidal pattern orientation angles is used to characterize tissue structural orientation in the SFD. The following section shows orientation angle and contrast maps on tissue structural orientation phantoms using both the Hilbert and the three-phase demodulation techniques.

3.3 *Scattering Orientation Experiment*

By rotating SFDI modulation patterns and acquiring diffuse reflectance maps at several projection angles, we can determine the orientation angle and magnitude of structures in biological tissue.[11] Therefore, if we wish to use the Hilbert technique to probe tissue orientation, we must verify that it can produce similar structural orientation contrast as three-phase SFDI. Figure 5 shows scattering orientation angle and contrast maps for the three-phase and Hilbert techniques at an AC spatial frequency of 0.2 mm^{-1}. The orientation angle of the structure being probed is determined by the angle at which minimum diffuse reflectance is detected. We see here that the average orientation angle for all three ROIs (shown in white boxes) is within 1 deg, which is well within our angular resolution of 5 deg.

To assess the degree to which the underlying structures are oriented, we used a normalized quantity known as the SOI, shown in Eq. (7).[11] Here, the SOI is determined by maximizing, for all projection angles, the reflectance taken at a given angle subtracted from the reflectance taken at the orthogonal projection angle, divided by the sum. The tissue structure orientation phantoms used consist of rectangular-shaped, pleated air filters having significant structural orientation, placed on top of a tissue-simulating phantom having minimal structural orientation

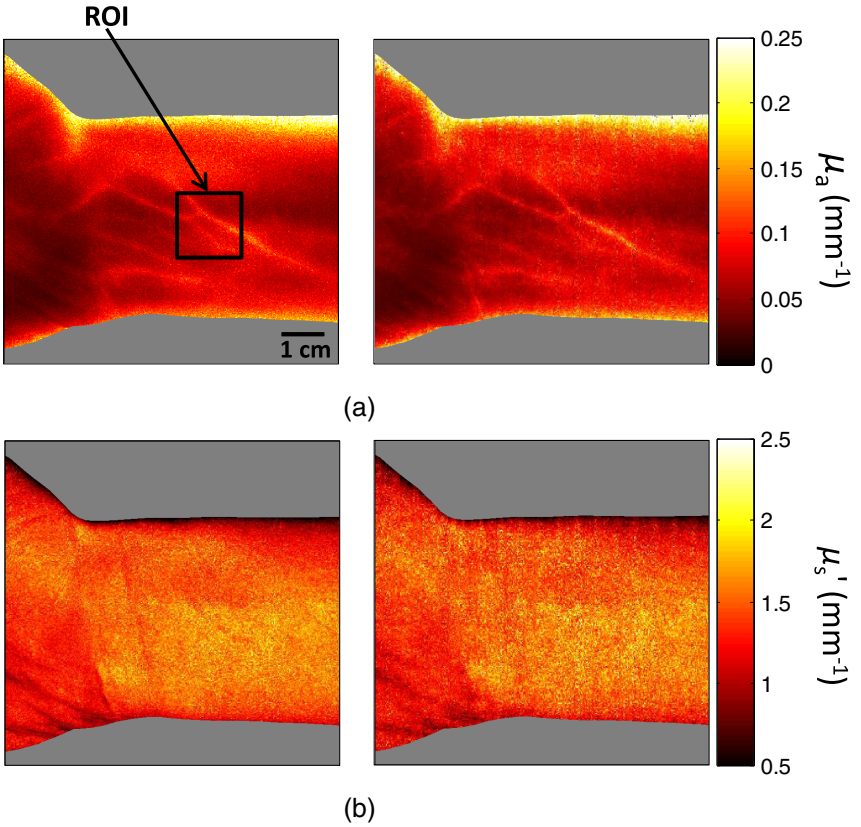

Fig. 4 *In vivo* optical property results taken from a human volar forearm. (a) Absorption (μ_a) and (b) reduced scattering (μ_s') coefficient maps derived from 4-frame, three-phase SFDI (left) and the 2-frame, Hilbert (right) demodulation techniques. For μ_a and μ_s', the difference in optical property calculations over the region of interest (ROI, shown in black box) is 0.2% and 0.15%, respectively.

$$\mathrm{SOI} = \max\left\{\frac{|g(\theta)| - |g(\theta+\pi/2)|}{|g(\theta)| + |g(\theta+\pi/2)|}\right\}. \quad (7)$$

Figure 5 shows SOI maps of tissue structural orientation phantoms using the three-phase (left column) and Hilbert (right column) demodulation techniques. In general, the SOI values obtained using the Hilbert technique are within 10% of those obtained using three-phase demodulation. In particular, the mean difference in the SOI is well within 10% for the three ROIs, and within 2% for two out of three of the ROIs. This demonstrates an overall agreement in SOI between results obtained using the Hilbert and three-phase techniques.

Since the characterization of structural orientation in SFDI uses multiple projection angles of sinusoidal patterns, several frames of data are required. In the case shown in Fig. 5, the angular resolution in orientation analysis is 5 deg. Since the orientation angle has a range of 0 to 180 deg, 36 projection angles were employed. Using the three-phase technique, this results in a total of 108 frames, whereas the Hilbert technique requires only 36 frames (one frame per projection angle). Thus, the Hilbert technique in this example increases imaging speed threefold over three-phase demodulation.

4 Discussion

One of the primary goals of quantitative tissue optical imaging is to separate scattering from absorption as quickly as possible to mitigate motion artifacts and enable the visualization of dynamic signals. This work introduces the Hilbert demodulation technique, which seeks to increase SFDI data acquisition speed while minimizing losses in information content. Our results suggest that the Hilbert technique is accurate in determining optical properties compared to the three-phase SFDI, using one-half the number of frames for two frequencies, and approaching one third the number of frames for many spatial frequencies. The tradeoff in image quality using the Hilbert approach comes primarily from ringing artifacts resulting from the finite length of the spatial modulation patterns. Our results demonstrate that these artifacts have a minor effect on our diffuse reflectance intensity measurements and thus optical property and SOI calculations. Taken at several wavelengths, these optical property values are used to determine the absolute concentration of chromophores such as oxy/deoxy-hemoglobin, which are direct measures of tissue function. In our *in vivo* forearm experiment (shown in Fig. 4), we obtained optical property values within 1% of the three-phase SFDI. The degree to which this difference in optical property values translates to differences in chromophore concentrations will vary depending on several parameters, including the chromophore spectra, the wavelengths and spatial frequencies used, and the inversion model employed to fit for μ_a and μ_s'. However, we expect that a 1% margin of error in μ_a and μ_s' calculations will be suitable for most applications.

Along with μ_a and μ_s', we have used the Hilbert technique to map structural orientation, showing that the SOI values derived from a structural orientation phantom are within 10% of the three-phase SFDI using one third the number of frames. These results suggest that the Hilbert technique could be used to rapidly map tissue structural orientation. However, it

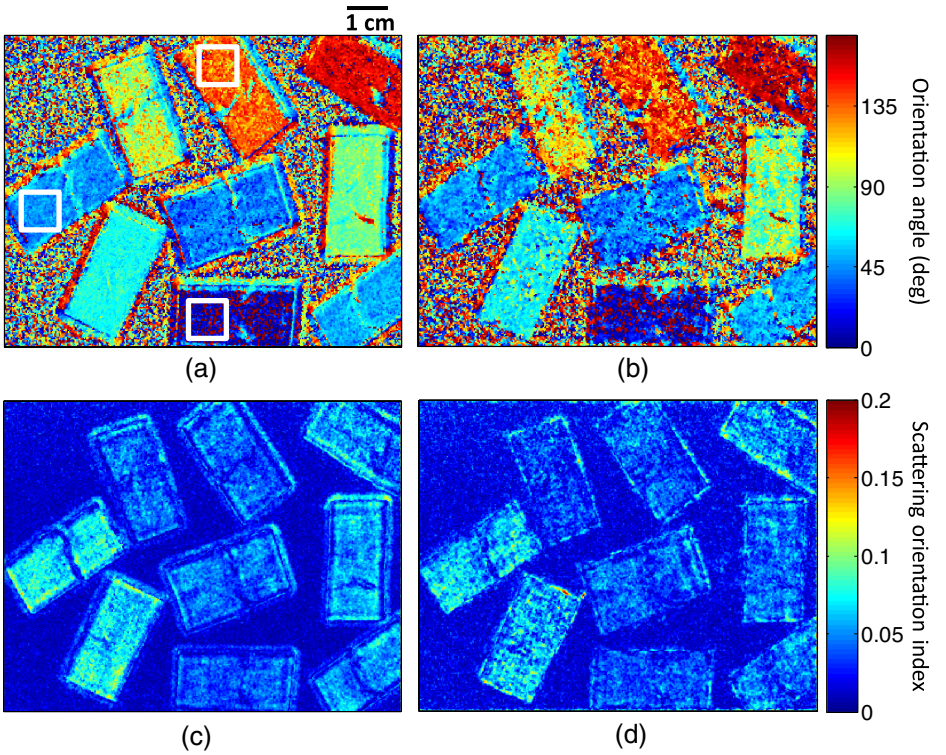

Fig. 5 Structural orientation results on structural orientation phantoms consisting of air filters with known structural anisotropy. Orientation angle maps derived from demodulated reflectance images using the (a) three-phase and (b) the Hilbert technique. Scattering orientation index (SOI) maps using (c) three-phase SFDI and (d) the Hilbert technique. ROIs were analyzed in three filters (white boxes). The difference mean orientation angle determined by the left, top, and bottom ROIs is 0, 1, and 0.75 deg, respectively. The difference in mean SOI in the left, top, and bottom ROIs between the Hilbert technique and conventional SFDI is 7.8%, 1.7%, and 0.27%, respectively.

is currently unclear how the difference in SOI values between the three-phase and Hilbert techniques will translate to quantifying structural orientation. The SOI is a qualitative index whose value depends on several parameters such as spatial frequency and wavelength. Moving forward, it will be important to evaluate the Hilbert technique in the context of quantitative orientation mapping, not just SOI. In the short term, there are enhancements that can be made that should improve orientation mapping using the Hilbert technique. For example, since the Hilbert technique uses fewer frames of data, there is more noise intrinsic to the demodulated images. The processing code used to spatially and angularly filter structural orientation data presented in Fig. 5 is optimized for three-phase SFDI, so tailoring this processing code to Hilbert demodulation could improve SOI mapping accuracy. Additionally, the use of a camera having less pixel noise could also improve SNR, and thus potentially improve SOI mapping.

In addition to reducing the number of frames needed, it should also be possible to further increase SFDI data acquisition speed using the Hilbert technique by exploring new modulation hardware that would otherwise be unavailable using three-phase demodulation. Since we only need a single, arbitrary phase for each AC modulation frequency, we can use a mechanical object such as a printed film in transmission geometry to modulate light. These devices have several benefits over electronic SLM's such as digital micromirror devices (DMDs) that are typically used in SFDI. For example, they have no refresh rate, so there is no longer a data acquisition time bottleneck due to this feature. sCMOS cameras have the ability to image at several thousand frames per second. However, scientific-grade DMDs have refresh rates in the order of single milliseconds. Therefore, in order to fully utilize these types of high-speed cameras, a DMD may not be the preferred modulation tool. Assuming adequate reflectance from the sample, allowing for millisecond or less frame rates, the use of a mechanical object for modulation could increase data acquisition speed by fivefold or more.

Ultimately, our goal is to acquire, process, and render optical property maps and SOI in real-time. Therefore, in addition to acquiring data, we must also process the data in real-time, which requires a certain amount of computation. In the case of three-phase demodulation, the mathematical operators in the demodulation formula are not computationally demanding, having linear or near linear computational complexities, denoted in Big O notation by $O(n)$. n in this case represents the number of digits used for each pixel, or simply each pixel, since the operation is linear. The fundamental difference between the Hilbert and three-phase demodulation techniques is the use of a 2-D FFT, which is applied to the entire image in the Hilbert technique. The FFT operation currently has a minimal computational demand of $O[n\log(n)]$ operations,[19] where n in this case represents the number of pixels. Assuming an image having 10^6 pixels (1000×1000), this translates to a computational demand of roughly an order of magnitude greater

than the linear, or "simple" operations. The three-phase formula consists of 12 simple operations for each pixel, whereas the Hilbert algorithm consists of 11 simple operations and two FFT's, resulting in a computational demand of roughly 31 simple operations for each pixel. Consequently, in theory, the Hilbert technique is expected to have approximately three times as much computational demand as the three-phase technique. By implementing the two techniques on images having the same pixel dimensions and bit depths as those shown in Figs. 2–4 in MATLAB on a desktop computer with a 3.06 GHz quad-core processor (Core i7-950, Intel Corporation, Santa Clara, California), we obtained computational times of 0.026 and 0.005 s for the Hilbert and three-phase techniques, respectively, which corresponds to a fivefold increase in computational time. With proper code optimization, the computational time of the Hilbert technique is not expected to prevent the implementation of a real-time SFDI platform.

In addition to mapping μ_a, μ_s', and SOI using fewer frames of data, the Hilbert demodulation technique has additional potential benefits that are not demonstrated here. One potential benefit to using the technique is an increase in profilometry data acquisition speed. As mentioned previously, the Hilbert transform allows for the determination of the phase angle of a modulated signal. The phase angle is derived by taking the inverse tangent of the ratio of the imaginary to the real component of the sum of the two terms $M(x,y)$ and $H(x,y)$, shown in Eqs. (3) and (6), respectively. This relationship is shown below in Eq. (8). Here, the concept of extracting phase angle is applied to images:

$$\text{phaseAngle}(x,y) = \tan^{-1}\frac{\text{imag}\{M(x,y)+iH(x,y)\}}{\text{real}\{M(x,y)+iH(x,y)\}}. \quad (8)$$

Modulated light can be used in the SFDI workflow to correct for artifacts related to surface curvature. Currently, SFDI employs a three-phase approach to compute phase angle maps, which are used to correct for surface curvature artifacts in reflectance data.[20] Using the Hilbert technique, it should be possible to perform a profilometry measurement using one frame of data instead of three, thus increasing profilometry data acquisition speed by threefold.

5 Conclusion

We have presented a new method for extracting spatial frequency information content from biological tissue which employs a 2-D Hilbert transform using a spiral phase function in 2-D Fourier space. This demodulation technique increases SFDI optical property data acquisition speed by two to threefold over conventional, three-phase demodulation, depending on the number of spatial frequencies used. Additionally, this technique increases tissue structural orientation data acquisition speed by threefold. We have applied this new approach to *in vivo* volar forearm data, from which μ_a and μ_s' maps were derived, showing agreement with the three-phase SFDI. We have also shown that the SOI values obtained from a structural orientation phantom using our new approach are comparable to those obtained using three-phase SFDI. Future work in instrumentation development geared toward optimizing the use of our new demodulation technique is expected to allow for the implementation of a real-time SFDI platform.

Acknowledgments

The authors gratefully acknowledge funding provided by the NIH NIBIB Biomedical Technology Research Center LAMMP: P41EB015890, NIH (grants: R21-EB014440, K01-DK-093603), the Military Medical Photonics Program, AFOSR Grant No. FA9550-08-1-0384, and the Beckman Foundation. Kyle P. Nadeau was supported by the BEST IGERT program funded by the National Science Foundation DGE-1144901. Bruce J. Tromberg and Anthony J. Durkin report patents owned by the University of California that are related to SFDI technology, and are co-founders of Modulated Imaging (MI), Inc., which has licensed SFDI from the University of California.

References

1. T. D. O'Sullivan et al., "Diffuse optical imaging using spatially and temporally modulated light," *J. Biomed. Opt.* **17**(7), 071311 (2012).
2. N. Dognitz and G. Wagnières, "Determination of tissue optical properties by steady-state spatial frequency-domain reflectometry," *Lasers Med. Sci.* **13**(1), 55–65 (1998).
3. F. Bevilacqua et al., "Quantitative analysis and imaging of subsurface heterogeneities using spatially structured illumination," in *OSA Technical Digest, Biomedical Topical Meetings*, pp. 677–679, OSA, Washington DC (2002).
4. D. J. Cuccia et al., "Modulated imaging: quantitative analysis and tomography of turbid media in the spatial-frequency domain," *Opt. Lett.* **30**(11), 1354–1356 (2005).
5. D. J. Cuccia et al., "Quantitation and mapping of tissue optical properties using modulated imaging," *J. Biomed. Opt.* **14**(2), 024012 (2009).
6. A. Yafi et al., "Postoperative quantitative assessment of reconstructive tissue status in a cutaneous flap model using spatial frequency domain imaging," *Plast. Reconstr. Surg.* **127**(1), 117–130 (2011).
7. A. J. Lin et al., "Spatial frequency domain imaging of intrinsic optical property contrast in a mouse model of Alzheimer's disease," *Ann. Biomed. Eng.* **39**(4), 1349–1357 (2011).
8. K. P. Nadeau et al., "Quantitative assessment of renal arterial occlusion in a porcine model using spatial frequency domain imaging," *Opt. Lett.* **38**(18), 3566–3569 (2013).
9. J. Q. Nguyen et al., "Effects of motion on optical properties in the spatial frequency domain," *J. Biomed. Opt.* **16**(12), 126009 (2011).
10. J. Vervandier and S. Gioux, "Single snapshot imaging of optical properties," *Biomed. Opt. Express* **4**(12), 2938–2944 (2013).
11. S. D. Konecky et al., "Imaging scattering orientation with spatial frequency domain imaging," *J. Biomed. Opt.* **16**(12), 126001 (2011).
12. N. E. Huang and S. S. Shen, *Hilbert-Huang Transform and Its Applications*, World Scientific, Hackensack, New Jersey (2005).
13. K. G. Larkin, "Natural demodulation of two-dimensional fringe patterns. II. Stationary phase analysis of the spiral phase quadrature transform," *J. OSA A.* **18**(8), 1871–1881 (2001).
14. K. G. Larkin, D. J. Bone, and M. A. Oldfield, "Natural demodulation of two-dimensional fringe patterns. I. General background of the spiral phase quadrature transform," *J. OSA A.* **18**(8), 1862–1870 (2001).
15. J. S. Chitode, *Digital Signal Processing*, Technical Publications, Pune, India (2008).
16. D. J. Cuccia, "Spatial Frequency Domain Imaging (SFDI): a technology overview and validation of an LED-based clinic-friendly device," *Proc. SPIE* **8254**, 825405 (2012).
17. F. Ayers et al., "Fabrication and characterization of silicone-based tissue phantoms with tunable optical properties in the visible and near infrared domain," *Proc. SPIE* **6870**, 687007 (2008).
18. J. Q. Nguyen et al., "Spatial frequency domain imaging of burn wounds in a preclinical model of graded burn severity," *J. Biomed. Opt.* **18**(6), 66010 (2013).
19. S. G. Johnson and M. Frigo, "A modified split-radix FFT with fewer arithmetic operations," *IEEE Trans.* **55**(1), 111–119 (2007).
20. S. Gioux et al., "Three-dimensional surface profile intensity correction for spatially modulated imaging," *J. Biomed. Opt.* **14**(3), 034045 (2009).

Kyle P. Nadeau received his BS in electrical and computer engineering from Northeastern University in Boston, Massachusetts, in 2011, and an MS in biomedical engineering at the University of California, Irvine, in 2013. He is currently an NSF IGERT fellow, pursuing his PhD in biomedical engineering at the University of California, Irvine, in the Wide-field Functional Imaging (WiFI) Laboratory. His main interest is in advanced spatial frequency domain techniques for quantitative tissue imaging spectroscopy.

Anthony J. Durkin is an associate professor at the Beckman Laser Institute (BLI) at the University of California, Irvine. His research is focused on the development and application of optical spectroscopic and quantitative wide-field imaging techniques to characterize superficial tissues *in-vivo*. He is codirector of the Wide-field Functional Imaging program at BLI. He holds his PhD in biomedical engineering from the University of Texas at Austin with emphasis on biomedical optics and spectroscopy.

Bruce J. Tromberg is the director of the Beckman Laser Institute and Medical Clinic (BLI) at the University of California, Irvine, and principal investigator of the Laser Microbeam and Medical Program (LAMMP), an NIH P41 National Biomedical Technology Center in the BLI. He is a professor with joint appointments in the departments of Biomedical Engineering and Surgery and has been a member of the UCI faculty since 1990.